UCLA
UCLA Previously Published Works

Title

Covariance J-resolved spectroscopy: Theory and application in vivo

Authors

Iqbal, Zohaib

Verma, Gaurav

Kumar, Anand

et al.

WILEY **NMR** IN BIOMEDICINE

RESEARCH ARTICLE

Covariance *J*-resolved spectroscopy: Theory and application *in vivo*

Zohaib Iqbal[1] | Gaurav Verma[1] | Anand Kumar[2,3] | M. Albert Thomas[1] (iD)

[1]Department of Radiological Sciences, University of California Los Angeles, Los Angeles, USA

[2]Department of Psychiatry, University of California Los Angeles, Los Angeles, USA

[3]Department of Psychiatry, University of Illinois at Chicago, Chicago, IL, USA

Correspondence
Michael Albert Thomas, 10945 Le Conte Avenue, Suit #3371, Los Angeles, California, USA.
Email: athomas@mednet.ucla.edu

Funding information
National Institute of Health R21, Grant/Award Number: NS080648-02; University of California–Los Angeles Dissertation Year Fellowship Award (2016–2017)

Magnetic resonance spectroscopy (MRS) is a powerful tool capable of investigating the metabolic status of several tissues *in vivo*. In particular, single-voxel-based ^{1}H spectroscopy provides invaluable biochemical information from a volume of interest (VOI) and has therefore been used in a variety of studies. Unfortunately, typical one-dimensional MRS data suffer from severe signal overlap and thus important metabolites are difficult to distinguish. One method that is used to disentangle overlapping resonances is the two-dimensional *J*-resolved spectroscopy (JPRESS) experiment. Due to the long acquisition duration of the JPRESS experiment, a limited number of points are acquired in the indirect dimension, leading to poor spectral resolution along this dimension. Poor spectral resolution is problematic because proper peak assignment may be hindered, which is why the zero-filling method is often used to improve resolution as a post-processing step. However, zero-filling leads to spectral artifacts, which may affect visualization and quantitation of spectra. A novel method utilizing a covariance transformation, called covariance *J*-resolved spectroscopy (CovJ), was developed in order to improve spectral resolution along the indirect dimension (F_1). Comparison of simulated data demonstrates that peak structures remain qualitatively similar between JPRESS and the novel method along the diagonal region ($F_1 = 0\,Hz$), whereas differences arise in the cross-peak ($F_1 \neq 0\,Hz$) regions. In addition, quantitative results of *in vivo* JPRESS data acquired on a 3T scanner show significant correlations ($r^2 > 0.86$, $p < 0.001$) when comparing the metabolite concentrations between the two methods. Finally, a quantitation algorithm, 'COVariance Spectral Evaluation of [1]H Acquisitions using Representative prior knowledge' (Cov-SEHAR), was developed in order to quantify γ-aminobutyric acid and glutamate from the CovJ spectra. These preliminary findings indicate that the CovJ method may be used to improve spectral resolution without hindering metabolite quantitation for *J*-resolved spectra.

KEYWORDS

covariance NMR, enhanced spectral resolution, human brain, J-resolved spectroscopy (JPRESS), Magnetic Resonance Spectroscopy (MRS), prior-knowledge fitting

1 | INTRODUCTION

For decades, ^{1}H NMR has been utilized to identify various chemical and biological structures. Application of this technique to medicine in the form of magnetic resonance imaging (MRI) and magnetic resonance spectroscopy (MRS) has greatly enhanced understanding of anatomical, functional, and metabolic processes *in vivo*. In particular, ^{1}H MRS has been used in the investigation of metabolism in the brain[1] and several other regions[2-5] using single-voxel based methods such as point-resolved spectroscopy (PRESS).[6] The PRESS technique localizes a volume of interest (VOI) and obtains a one-dimensional (1D) spectrum from this region that can be analyzed and quantified using a variety of methods. Biochemicals associated with

Abbreviations used: 1D, One-dimensional; 2D, Two-dimensional; Asp, Aspartate; Ch, Choline; CovJ, Covariance J-resolved spectroscopy; Cov-SEHAR, COVariance Spectral Evaluation of [1]H Acquisitions using Representative prior knowledge; Cr3.0, Creatine 3.0; Cr3.9, Creatine 3.9; FT, Fourier transformation; GABA, γ-aminobutyric acid; Gln, Glutamine; Glu, Glutamate; Glx, Glutamate + Glutamine; GSH, Glutathione; JPRESS, J-resolved spectroscopy; Lac, Lactate; mI, myo-Inositol; MM, Macromolecules; NAA, N-acetyl aspartate; NAA-asp, N-acetyl aspartate aspartyl; NOESY, Nuclear Overhauser effect spectroscopy; STI, soybean trypsin inhibitor; PRESS, Point-resolved spectroscopy; SBW, Spectral bandwidth; SVD, Singular value decomposition; TOCSY, Total correlation spectroscopy; VOI, Volume of Interest.

metabolic processes are referred to as metabolites and concentrations of these molecules can be monitored non-invasively using MRS to study both healthy and patient cohorts. For example, the most prominent neurotransmitter in the human brain, glutamate (Glu), has been studied extensively using several different MRS methods.[7]

Unfortunately, certain resonances, including Glu, glutamine (Gln), γ-aminobutyric acid (GABA), and glutathione (GSH), overlap with other metabolic signals and thus accurate metabolite quantitation may be hindered even when implementing prior-knowledge-based quantitation.[8] Prior-knowledge-based quantitation refers to a methodology that obtains a basis spectrum for each individual metabolite, through either experimental acquisition or simulation. Acquired data are then modeled using a linear combination of these basis spectra to yield metabolite concentration values. One method that is capable of overcoming the disadvantage of overlapping resonances is a spectral editing technique utilizing MEGA pulses.[9] This method relies on saturating or inverting certain signals and then subtracting spectra to yield a final edited spectrum. Therefore, accurate quantitation of a single metabolite can be accomplished in this manner.

Another solution for disentangling overlapping signals is to acquire a second spectral dimension.[10] By acquiring an additional dimension, information based on the coupling of various resonances is also acquired alongside chemical shift information. Several two-dimensional (2D) MRS methods have been implemented successfully *in vivo*[11-16] and have been used for metabolite quantitation. The PRESS localized single-voxel J-resolved spectroscopy (JPRESS) method[11-13,16] is one 2D tool that was developed by adding a time increment, Δt_1, into a standard PRESS sequence. This time increment encodes the indirectly acquired temporal dimension, t_1, and may be transformed into the indirect spectral dimension, F_1, through the use of a Fourier transformation. The main disadvantage of the JPRESS method is that acquisition time is directly proportional to the number of t_1 points acquired. Also, since the number of t_1 points is inversely proportional to the spectral resolution, compromise between acquisition duration and spectral resolution becomes a necessity for recording high-quality spectra in a clinically feasible time. While the t_1 dimension can be zero-filled to improve spectral resolution, this method is notorious for introducing ringing artifacts along the F_1 domain.[17]

Covariance NMR[18,19] is another method implemented for improving resolution along the indirect spectral dimension and does not introduce the same ringing artifacts into the 2D spectra as zero-filling does. This technique has been utilized for a variety of different 2D experiments, primarily total correlation spectrosocpy (TOCSY) and nuclear Overhauser effect spectroscopy (NOESY) experiments,[20-22] and has even been applied to multi-nuclear acquisitions.[23,24] Covariance NMR replaces the second Fourier transformation applied to the t_1 dimension with a covariance transformation. The new F_1 dimension will then have the same spectral resolution as the direct spectral dimension, F_2. Although numerous applications have been described in NMR, covariance NMR has not been as widely implemented *in vivo*. This study focuses on describing covariance NMR theory applied to the JPRESS technique. This novel method, called covariance J-resolved spectroscopy (CovJ), is compared with the standard JPRESS method both qualitatively using simulations and quantitatively using *in vivo* J-resolved acquisitions from the human brain at 3T.

2 | METHODS

2.1 | Covariance NMR theory

Data acquired from a 2D spectroscopy experiment are stored as time-domain data and may be represented as a 2D matrix, $a(t_2, t_1)$, where t_2 is the directly acquired dimension and t_1 is the indirectly acquired dimension. In classical 2D Fourier transformation (FT) NMR, both dimensions would undergo Fourier transformation, yielding 2D spectral information given by a final matrix $S(F_2, F_1)$. The spectral resolution is dictated by the number of points acquired in both the direct dimension (N_2) and the indirect dimension (N_1), as well as the corresponding spectral bandwidths for both dimensions (SBW_2 and SBW_1) through the following relationships: SBW_2/N_2 and SBW_1/N_1. Due to the fact that acquisition duration is proportional to N_1, N_1 is always less than N_2 for in vivo 2D experiments. In many in vivo cases, N_1 may be a factor of 10 smaller than N_2, leading to poor resolution along the indirect spectral dimension. While spectral resolution may be improved by decreasing SBW_1, a large SBW_1 aids in suppressing water tail signal and reducing T_2 weighting of metabolites. Covariance transformation replaces the FT operation applied to the t_1 dimension, resulting in enhanced spectral resolution with no penalty on acquisition time.[18,19]

First, the acquired data matrix, $a(t_2, t_1)$, is Fourier transformed along the direct dimension to yield $A(F_2, t_1)$. The new 2D spectral matrix is then computed by identifying the relationship between the t_1 free induction decays (FIDs) at every F_2 point using the following:

$$ \mathcal{C}_{ij} = \frac{1}{N_1 - 1} \sum_{k=1}^{N_1} \left[A(i, k) - \overline{A}(i) \right] \left[A(j, k) - \overline{A}(j) \right] \tag{1} $$

Above, i and j are both used to index the F_2 dimension ($i = 1, 2, 3, \ldots, N_2$ and $j = 1, 2, 3, \ldots, N_2$), k is used to index the t_1 dimension ($k = 1, 2, 3, \ldots, N_1$), $\overline{A}(i)$ is the average of all k values at a single point i, and finally $\overline{A}(j)$ is the average of all k values at a single point j. For many 2D experiments, only the real values (Re) are used when computing $\mathcal{C}$, because the imaginary (Im) signals usually provide minimal additional information. Each element in $\mathcal{C}_{ij}$ in Equation 1 is representative of how well points i and j are related along t_1. For example, if both terms have a strong relationship, $|\mathcal{C}_{ij}|$ will be large. However, if points i and j are unrelated, such as if these points correspond to different metabolites or noisy spectral regions, then $|\mathcal{C}_{ij}|$ will be close to zero. Since the second dimension is constructed through Equation 1, the spectral resolution and SBW along the new indirect dimension are identical to the spectral resolution and SBW along the direct dimension. Therefore, this new indirect dimension may be referred to as F_2', and the covariance matrix is then $\mathcal{C}(F_2, F_2')$. As previously described,[19] S can be calculated from $\mathcal{C}$ by applying a matrix square-root operation,

$[]^{1/2}$, and multiplying by an appropriate scaling factor, α: $S = \alpha\left[\mathcal{C}\right]^{1/2}$. The constant α is dependent upon the 2D experiment performed, and can be calculated either theoretically[19] or directly from the data.

While Equation 1 provides a direct method for the computation of S, a more efficient method for calculating the 2D covariance spectrum is to use a singular value decomposition (SVD) on the normalized $A(F_2, t_1)$ matrix.[22] Similarly to Equation 1, normalization is performed by subtracting the average t_1 values for each individual F_2 point to yield $\tilde{A}(F_2, t_1)$. After normalization, it is possible to perform SVD on the resulting $\tilde{A}$ matrix to yield an N_2xN_2 unitary matrix (U), an N_2xN_1 rectangular diagonal matrix (W), and an N_1xN_1 unitary matrix (V).[22] From Equation 1, it can be shown that $\mathcal{C}$ is essentially $\tilde{A} \cdot \tilde{A}^\mathsf{T}$, where $^\mathsf{T}$ is the transpose operator, and therefore $\mathcal{C}$ can be represented as the following:

$$\mathcal{C} = U \cdot W \cdot V^\mathsf{T} \cdot V \cdot W \cdot U^\mathsf{T} \tag{2}$$

$$\mathcal{C} = U \cdot W^2 \cdot U^\mathsf{T} \tag{3}$$

Finally, knowing that S can be found by taking the matrix square root of $\mathcal{C}$:

$$S = U \cdot W \cdot U^\mathsf{T} \tag{4}$$

The SVD method is used preferentially for calculating S, since this technique has been shown to be more computationally efficient than Equation 1.[22]

2.2 | JPRESS and covariance JPRESS processing

Acquisitions of J-resolved spectra are typically performed by introducing a time increment, Δt_1, into the standard PRESS pulse sequence. This increment can be either incorporated symmetrically about the last 180° pulse (90° –180° –$\frac{t_1}{2}$–180° –$\frac{t_1}{2}$–read) or inserted entirely in between the two 180° pulses (90° –180° –t_1–180° –read). The former method starts recording the FID at the echo time and is referred to as the half-echo sampling scheme, whereas the latter method starts recording the FID immediately following the last 180° pulse and is called the maximum-echo sampling scheme.[25] It has previously been shown that the maximum-echo sampling scheme is capable of enhanced sensitivity[16,26] compared with the half-echo sampling method. For all processing, simulation, and in vivo details, mention of the JPRESS experiment refers to the maximum-echo sampled JPRESS acquisition.

First, data are acquired using typical JPRESS acquisition parameters: TR/TE = 2500/30 ms, t_2 points (N_2) = 2048, t_1 points (N_1) = 100, SBW_2 = 2000 Hz, SBW_1 = 1000 Hz, and Δt_1 = 1 ms. Importantly, the data are used to compose an acquisition matrix, $a(t_2, t_1)$, which is subsequently Fourier-transformed along the direct dimension to yield $A(F_2, t_1)$. Figure 1 displays the general processing steps for both JPRESS and covariance JPRESS (CovJ) spectra. In order to obtain the standard JPRESS spectrum from this matrix, the chemical shift must first be refocused by applying a phase multiplication term to $A(F_2, t_1)$[16]:

$$\tau_1(F_2, t_1) = \exp(-2I\pi V_2 V_1^\mathsf{T}) \tag{5}$$

where $I = \sqrt{-1}$, V_2 is an $N_2 \times 1$ vector indexing the F_2 dimension from −1000 to 1000 Hz, and V_1 is an $N_1 \times 1$ vector indexing the t_1 dimension from 0–99 ms. The matrix A is then multiplied by the phase modulation matrix, τ_1, in an elementwise manner to refocus the chemical shift along the indirect dimension: $A \odot \tau_1$, where $\odot$ denotes elementwise multiplication. Finally, this corrected matrix can then be Fourier-transformed along the indirect dimension to yield $S(F_2, F_1)$, which is the standard N_2xN_1 JPRESS spectrum. Due to the phase multiplication process, the observed spectral bandwidth in the indirect dimension becomes half (±250 Hz) of the acquired SBW_1 (1000 Hz).

The CovJ approach also begins with the matrix $A(F_2, t_1)$. However, the covariance spectrum is computed using both the real and imaginary components of $\tilde{A}(F_2, t_1)$ as follows:

$$S_R = [Re(\tilde{A}) \cdot Re(\tilde{A}^\mathsf{T})]^{1/2} = U_R \cdot W_R \cdot U_R^\mathsf{T} \tag{6}$$

$$S_I = [Im(\tilde{A}) \cdot Im(\tilde{A}^\mathsf{T})]^{1/2} = U_I \cdot W_I \cdot U_I^\mathsf{T} \tag{7}$$

$$S' = S_R + S_I \tag{8}$$

Equation 6 utilizes SVD on the real component of $\tilde{A}$, $Re(\tilde{A})$, in order to obtain U_R and W_R, whereas Equation 7 performs SVD on the imaginary component of $\tilde{A}$, $Im(\tilde{A})$, to yield U_I and W_I. In order to display the CovJ results in the same manner as the JPRESS results, a different phase-tilting term must be applied to S' in the mixed frequency–time domain. Therefore, S' is first inverse Fourier-transformed along the indirect dimension to yield $S'_m(F_2, t'_2)$. Then, the following phase modulation matrix is applied to S'_m:

$$\tau_2(F_2, t'_2) = \exp(-I\pi V_2 V_3^\mathsf{T}) \tag{9}$$

Above, V_2 is the same vector used in Equation 5 and V_3 is an $N_2 \times 1$ vector indexing the time increment, accounting for the increased number of points (0–2047 ms). Phase tilting is performed by the following operation: $S'_m \odot \tau_2$. Finally, the matrix is brought back into the spectral domain using a Fourier transformation, yielding the final $N_2 \times N_2$ covariance spectrum, $S_{cov}(F_2, F'_1)$. Once again, due to the phase tilting method, the spectral
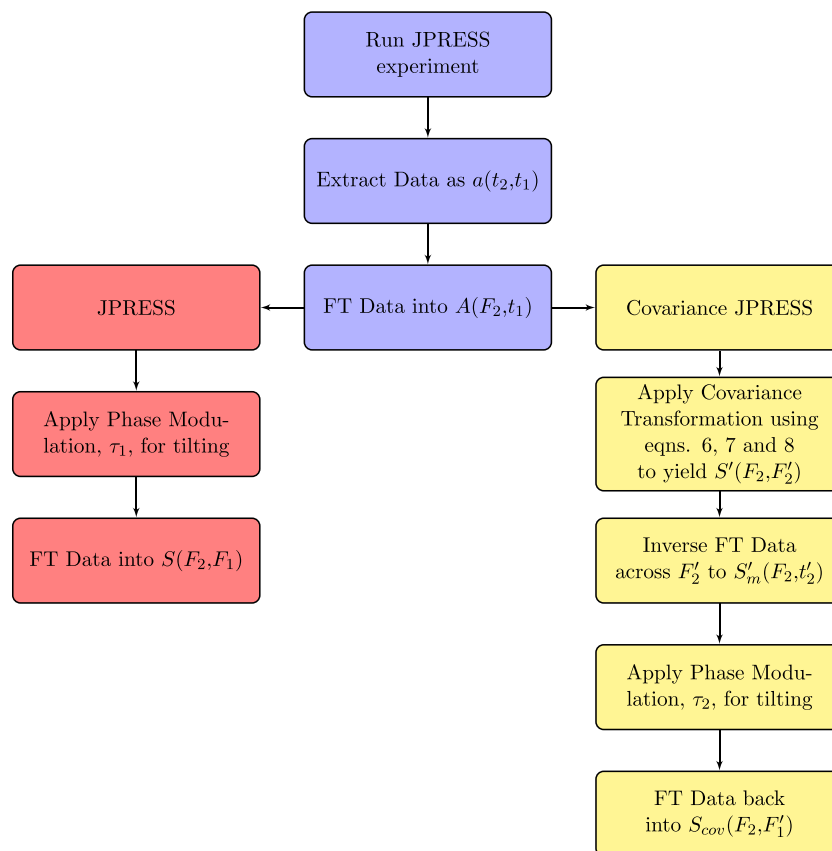
FIGURE 1 A flow chart outlining the steps for JPRESS (red) and covariance JPRESS (yellow) processing is shown. After data acquisition and extraction, the data are Fourier-transformed (FT) into the (F_2, t_1) domain. For JPRESS, the data are then multiplied with a 2D phase modulation term to refocus chemical shift. The data are then subsequently brought into the (F_2, F_1) domain for display/quantitation. For covariance JPRESS, a covariance transformation is applied to the data. Afterwards, a similar tilting process is performed to yield CovJ data

bandwidth of the F_1' dimension is ± 500 Hz. Thus, the observed indirect spectral resolution for JPRESS is 5 Hz/pt and that for CovJ is 0.49 Hz/pt. The CovJ results can be represented by real positive and negative values exclusively; however, in order for fair comparison between JPRESS spectra, the data are displayed and quantified in magnitude mode.

2.3 | Simulation

In order to demonstrate the application of the CovJ method and compare the CovJ results qualitatively with the JPRESS method, metabolite spectra were obtained using the general approach to magnetic resonance mathematical analysis (GAMMA) simulation[27] with the following simulation parameters: $B_0 = 2.89$T, TE = 30 ms, $\Delta t_1 = 1$ ms, t_2 points (N_2) = 2048, t_1 points (N_1) = 100, $SBW_2 = 2000$ Hz, and $SBW_1 = 1000$ Hz. Previously reported chemical shift and coupling values[28] were used to simulate the following metabolites: aspartate (Asp), choline (Ch), creatine 3.0 (Cr3.0), creatine 3.9 (Cr3.9), GABA, Gln, Glu, GSH, lactate (Lac), myo-Inositol (mI), and N-acetyl aspartate (NAA). Exponential line-broadening factors were introduced to each metabolite to simulate in vivo acquisition, resulting in linewidths of 7.5 Hz. The CovJ technique was applied to each metabolite individually and compared with the JPRESS displays. In addition, the CovJ and JPRESS methods were applied to a composite spectrum, which was created by combining the metabolites with the following relative concentrations: 1 mM Asp, 2 mM Ch, 6 mM Cr3.0, 6 mM Cr3.9, 1 mM GABA, 3 mM Gln, 7 mM Glu, 1 mM GSH, 2 mM Lac, 5 mM mI, and 8 mM NAA. To provide a fair comparison, zero-filling was also applied to the JPRESS results, leading to a final $SBW_1 = 0.5$ Hz/pt, which was equivalent to the CovJ indirect spectral resolution. Finally, different spectra were simulated using the same process, except that Glu/(Glu+Gln) ratios, also referred to as Glu/Glx ratios, were altered. All other metabolites were held constant, while the Glu% was varied in order to observe the effects of concentration on cross-peak structure for the CovJ method.

2.4 | In vivo acquisition and quantitation

A total of 24 healthy, elderly volunteers (mean age = 64.7 years old) were scanned on a 3T Siemens Trio scanner (Siemens Healthcare, Erlangen, Germany). The MR protocol and written consenting procedure were both approved by the Institutional Review Board at the University of California–Los Angeles. First, T_1-weighted images were obtained in order to localize the VOI for the MRS acquisition. Next, the VOI was localized

using PRESS[6] in the medial, frontal gray matter for each healthy volunteer, and a 2D JPRESS acquisition was performed on this region using due following scan parameters: TR/TE = 2500/30 ms, $\Delta t_1 = 1$ ms, t_2 points (N_2) = 2048, t_1 points (N_1) = 100, averages = 4, $SBW_2 = 2000$ Hz, $SBW_1 = 1000$ Hz, and voxel size = 2.5×2.5 x 2.5cm^3. It is important to note that, since both JPRESS and CovJ are obtained by using the same data set, $a(t_2, t_1)$, the acquisition times for both methods are identical. Water suppression was enabled using water suppression enhanced through T1 effects (WET) pulses.[29] Due to the voxel size, some white matter was also present in the VOI, however the voxel contained mostly gray matter for all volunteers. As mentioned above, the 2D JPRESS data were acquired using the maximum echo sampling scheme, which starts readout immediately following the last crusher gradient.[16] Using a 32 GB RAM workstation equipped with an Intel Core i7 processor, the total time for data extraction and processing (JPRESS and CovJ methods) for each data set was approximately 13 s in MATLAB version R2013A.

Afterwards, both the JPRESS and CovJ results were quantified using peak integration for the spectral regions corresponding to NAA, Cr3.0, Ch, mI, Lipids + macromolecules (MM), and Glu+Gln (Glx). The following 2D spectral ranges, (F_2 limits in ppm, $\pm F_1$ in Hz) were used for JPRESS quantitation: (1.2–1.6, ±10) for Lipids + MM, (1.9–2.1, ±10) for NAA, (2.2–2.5, ±20) for Glx, (2.9–3.1, ±10) for Cr3.0, (3.1–3.3, ±10) for Ch, and (3.4–3.6, ±20) for mI. The same F_2 regions were used for the CovJ quantitation, however the F'_1 regions were adjusted: ±7.3 Hz for Lipids + MM, ±7.3 Hz for NAA, ±12.7 Hz for Glx, ±7.3 Hz for Cr3.0, ±7.3 Hz for Ch, and ±12.7 Hz for mI. Quantitative results were tabulated as both concentration values and as ratios with respect to Cr3.0 (/Cr3.0) for statistical comparisons.

In order to quantify GABA and Glu from the CovJ spectra, a quantitation method similar to prior-knowledge fitting (ProFit)[30,31] was developed. Instead of fitting concentration values linearly, this algorithm, termed 'COVariance Spectral Evaluation of ^{1}H Acquisitions using Representative prior-knowledge' (Cov-SEHAR), used non-linear fitting to determine concentration values. First, the data were frequency-drift and phase-corrected based on NAA, Cr3.0 and PCh prior knowledge, as previously described.[32] Next, a masking matrix, $\mathcal{M}$, was constructed to highlight the CovJ spectral regions of interest for the $S'(F_2, F'_2)$ matrix (untilted CovJ spectrum). In particular, $\mathcal{M}$ nulled the signal outside the 2.15–2.65 ppm spectral region and also nulled the diagonal signal so that the fitting would emphasize the off-diagonal peaks at $|J| \geq 4$ Hz. Representative prior knowledge was simulated using GAMMA,[27] and the basis set contained NAA, Cr3.0, PCh, GABA, Gln, Glu, and GSH. Even though Glu and GABA were of primary interest, the other metabolites were necessary in order to fit the background and overlapping signals. The following objective function was minimized using the lsqnonlin function in MATLAB:

$$\left\| \mathcal{M} \odot \left\{ S' - \text{Covar}\left[\sum_{m=1}^{m} \bar{\mathcal{C}}_m R_m \odot e^{-lb_m} \odot e^{-d_m} \right] \right\} \right\|_2^2 \tag{10}$$

Above, S' is the data acquired in the covariance domain, m is the number of metabolites included in the basis set, $\bar{\mathcal{C}}_m$ is the concentration of metabolite m, and R_m is the basis set in the (t_2, t_1) domain of metabolite m. In addition, each metabolite was given a line-broadening factor (lb_m) and a T_2 decay factor (d_m) in the form of matrices. The Covar operation above transforms the (t_2, t_1) data into the (F_2, F'_2) domain, which allows for direct comparison with the acquired data. Finally, $\mathcal{M}$ is applied to yield the final residual between the original data and the fit. For comparison purposes, ProFit was used to fit the JPRESS data using the same basis set and processing steps described previously.[30] The metabolite ratios of GABA/Cr3.0 and Glu/Cr3.0 were compared between the JPRESS and CovJ fitting methods.

2.5 | Statistical analysis

Statistical comparisons focused on investigating the similarities and differences between the quantitative JPRESS and CovJ in vivo results. First, mean and standard deviation (std) values were calculated for all metabolite ratios. Next, the coefficient of variation (CV) was calculated using $CV\% = 100(std/mean)$ for each metabolite ratio. Additionally, the metabolite ratios from the JPRESS and CovJ quantitation were compared directly using a Student's t-test for each metabolite. A Bonferroni correction[33] was used to account for multiple testing, and significance was determined as $p < 0.01$. Concentration values were not compared in the same manner, but were instead correlated with each other, yielding correlation coefficients (r and r^2).
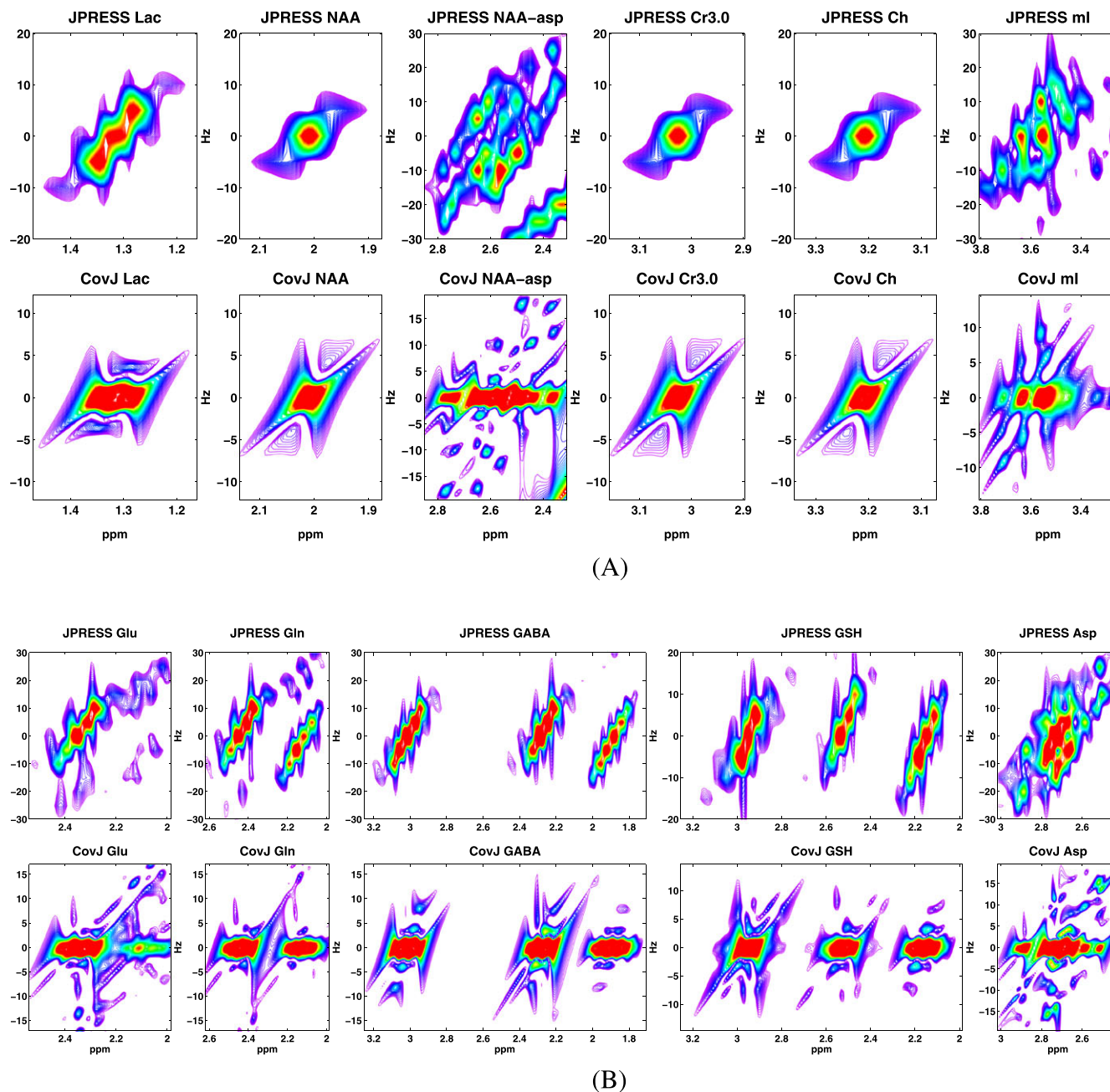
3 | RESULTS

3.1 | Simulation results

Figure 2 displays the results for the JPRESS and CovJ processing steps for several different metabolites. Singlet resonances, including the NAA, Cr3.0, and Ch singlets, show fairly similar results when comparing both methods. Mainly, the higher amplitude signal is concentrated at a single point for each respective singlet resonance ($F_2 = 2.01, 3.01, 3.2$ ppm and $F_1/F'_1 = 0$ Hz). The CovJ singlets slightly differ in peak structure, and added peaks can be seen slightly above ($F'_1 = 4$ Hz) and below ($F'_1 = -4$ Hz) each singlet. These additional peaks can be attributed directly to the points lying on the slopes of each singlet.

For multiplet resonances such as mI, Glu, Gln, GABA, GSH, and Asp, several differences are seen between the JPRESS and CovJ spectra. One of the apparent discrepancies is that the CovJ spectra collapse the off-diagonal signal ($F_1/F'_1 \neq 0$ Hz) on to the diagonal ($F_1/F'_1 \neq 0$ Hz). This is due to the fact that point i along F_2 has the strongest relationship with itself, according to Equation 1. Thus, the highest signal amplitude remains on

FIGURE 2 The peak structures resulting from both JPRESS and CovJ methods are shown. In A, the displayed metabolites include lactate (Lac), the N-acetyl aspartate singlet (NAA), the NAA aspartyl group (NAA-asp), creatine (Cr3.0), choline (Ch), and myo-Inositol (mI). Similarly, B, includes glutamate (Glu), glutamine (Gln), γ-aminobutyric acid (GABA), glutathione (GSH), and aspartate (Asp). In general, peak structures at F_1 and $F'_1 = 0$ Hz are very similar, while off-diagonal peaks (F_1 and $F'_1 \neq 0$ Hz) have different peak structures

$F'_1 \neq 0$ Hz for the CovJ spectra, which is not the case for several J-resolved metabolic signals. However, a potential benefit of the CovJ method is the fine peak structures that form for many multiplets. For example, the CovJ spectrum of the NAA aspartyl group (NAA-asp) shows well-defined peaks representative of the multiplet signal arising in the 2.4–2.8 ppm region. Glu and Gln also display unique peak structures located at $F'_1 = \pm 15$ Hz. Therefore, while peak shape and structure are not identical for the two data sets, the unique peaks originating from the covariance method may still aid in identifying particular resonances.

In addition to comparing individual resonance signals, simulated JPRESS, zero-filled JPRESS, and CovJ spectra containing 11 metabolites with typical in vivo concentrations were also compared, as seen in Figure 3. At first glance, it appears that both the JPRESS and CovJ spectra are a linear combination of the metabolites scaled to their respective concentration values. It is well known that this is indeed the case regarding JPRESS spectra, and only peak amplitudes are affected when metabolite concentrations are altered, while peak structures remain as expected. This fact is also demonstrated in Figure 4 for Glu and Gln off-diagonal peaks. However, upon inspection of the CovJ off-diagonal peaks in the 2.2–2.5 ppm region, it is clear that Glu/Glx ratios affect peak structure in addition to peak amplitude. Specifically for Glu/Glx ratios, as the concentration of Glu
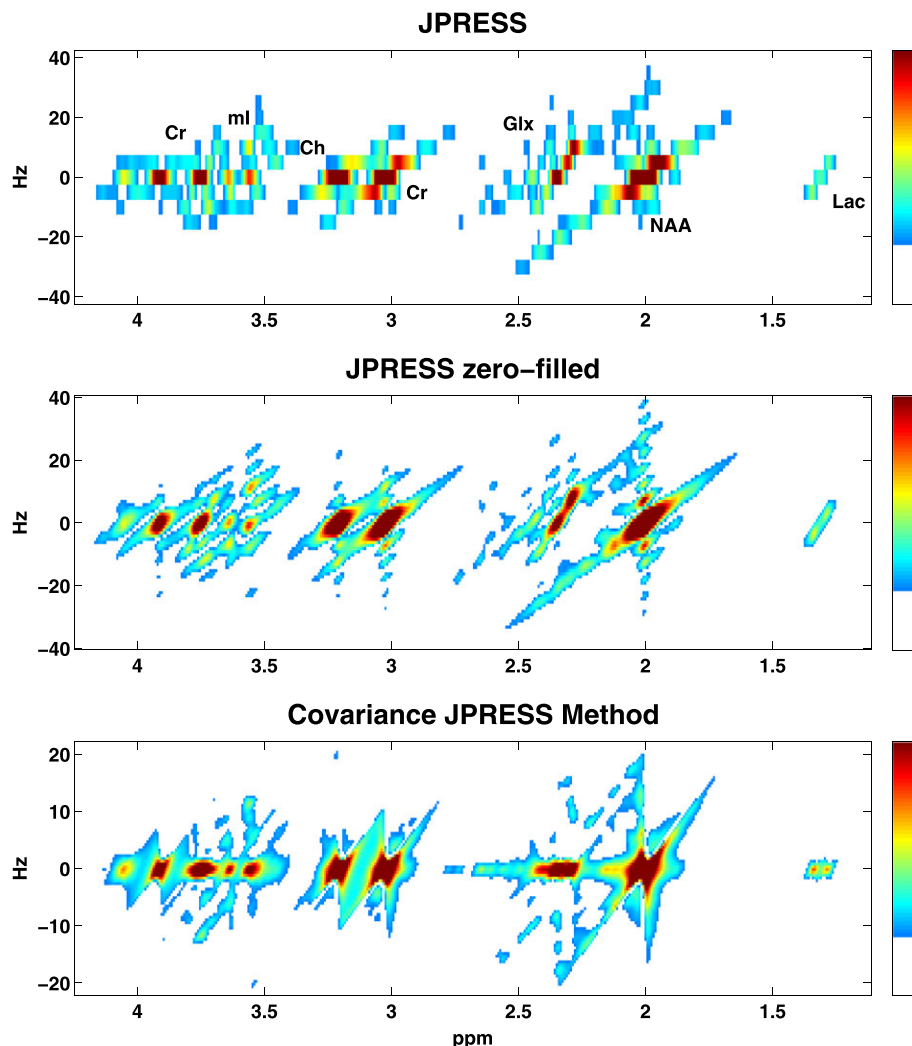
FIGURE 3 Simulated spectra using the JPRESS (top) and covariance JPRESS (bottom) methods are displayed. The zero-filled JPRESS spectrum (middle) is also shown to allow for direct comparison between spectra with equivalent spectral resolution. Since CovJ spectra do not have a true indirect spectral dimension, the data are displayed in a similar manner to the JPRESS F_1 dimension. Due to zero-filling, ringing across the F_1 dimension is apparent in the middle spectrum

decreases in relation to Glu+Gln, the two off-diagonal peaks inside the black boxes separate, as seen in Figure 4. This implies that CovJ off-diagonal peaks are non-linear representations of metabolite concentrations, and therefore peak structure is inherently different between the two methods.

3.2 | In vivo results

A maximum-echo sampled acquisition, as described above, was performed on 24 volunteers, and both JPRESS and CovJ data were obtained from this experimental data. Figure 5 shows localization of the medial, frontal gray region and also displays spectra from both JPRESS and CovJ techniques from a healthy, 63 year old volunteer. Contour plots of the two methods show qualitatively similar features, whereas improvement in spectral resolution is evident when comparing the true resolution spectra. For the CovJ spectra, off-diagonal peaks are displayed clearly for Glx and mI. In addition to the 2D spectral displays, 1D spectra can also be extracted from the CovJ data, as seen in Figure 6. These 1D spectra show unique line shapes attributed to the diagonal and off-diagonal peaks for Glx as well as mI, and provide a more detailed display of these peak intensities.

JPRESS and CovJ spectra were also quantified using peak integration, yielding both metabolite concentrations and ratios with respect to Cr3.0 for the major metabolites of interest. Metabolite ratio means and *CV%* values are displayed in Table 1. For both methods, *CV%* was relatively similar and most metabolites had *CV%* below 20%, with the exception of Lipids+MM. The mean values for both methods were nearly identical, however mI was significantly higher for the CovJ results (p < 0.001). Upon inspection of mI in Figure 5, it is apparent that this elevation arises due to the off-diagonal peaks that form at $F'_1 = \pm 7$ Hz for the CovJ spectra. This difference in mI/Cr3.0 does not necessarily imply that the CovJ method was ineffective at properly quantifying mI for each volunteer, however.

Examining the concentration values for both methods provides insight into how well the CovJ method detects metabolites on a volunteer-by-volunteer basis relative to the JPRESS method. The correlation values (r^2) between the CovJ and JPRESS peak integral concentrations
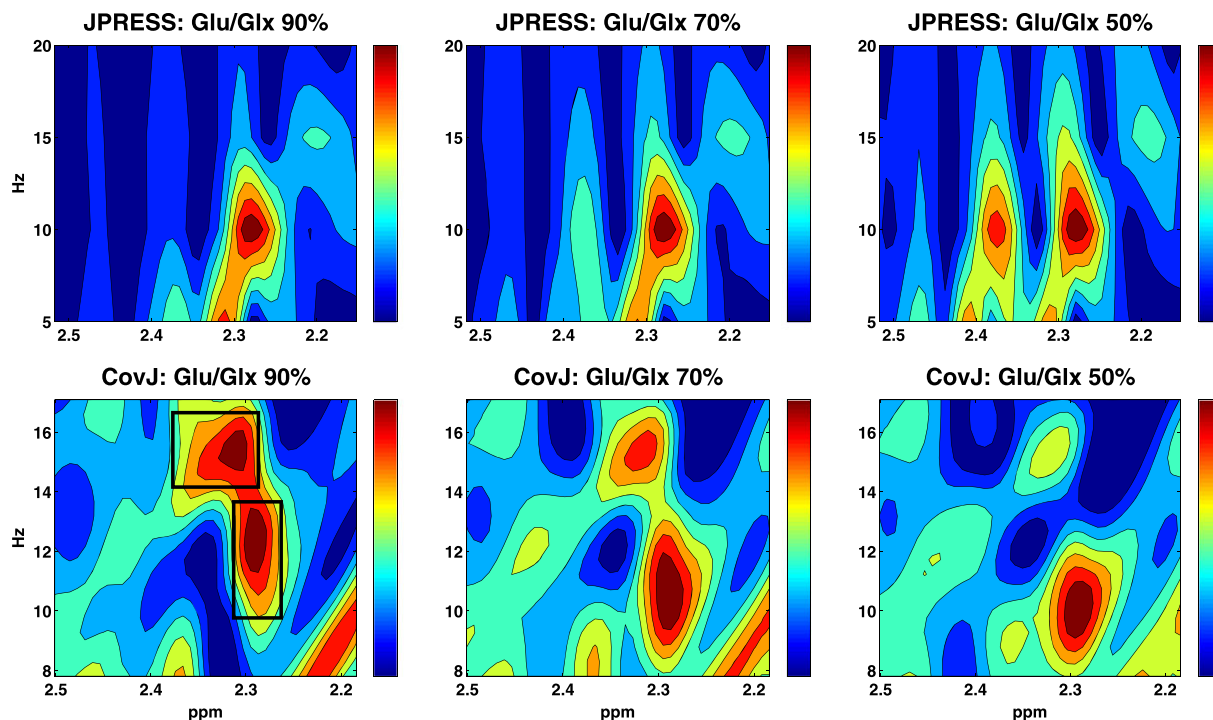
FIGURE 4 Spectral regions are shown for both JPRESS and CovJ methods, corresponding to Glx peaks. Glu and Gln levels were varied while all other metabolites were held at constant concentration values. As Glu/Glx ratios decrease, the peak amplitude varies while the overall peak structures remain identical for the JPRESS method. CovJ results, however, demonstrate that when Glu/Glx ratios decrease peak structure is also affected, as highlighted by the peaks in the black boxes
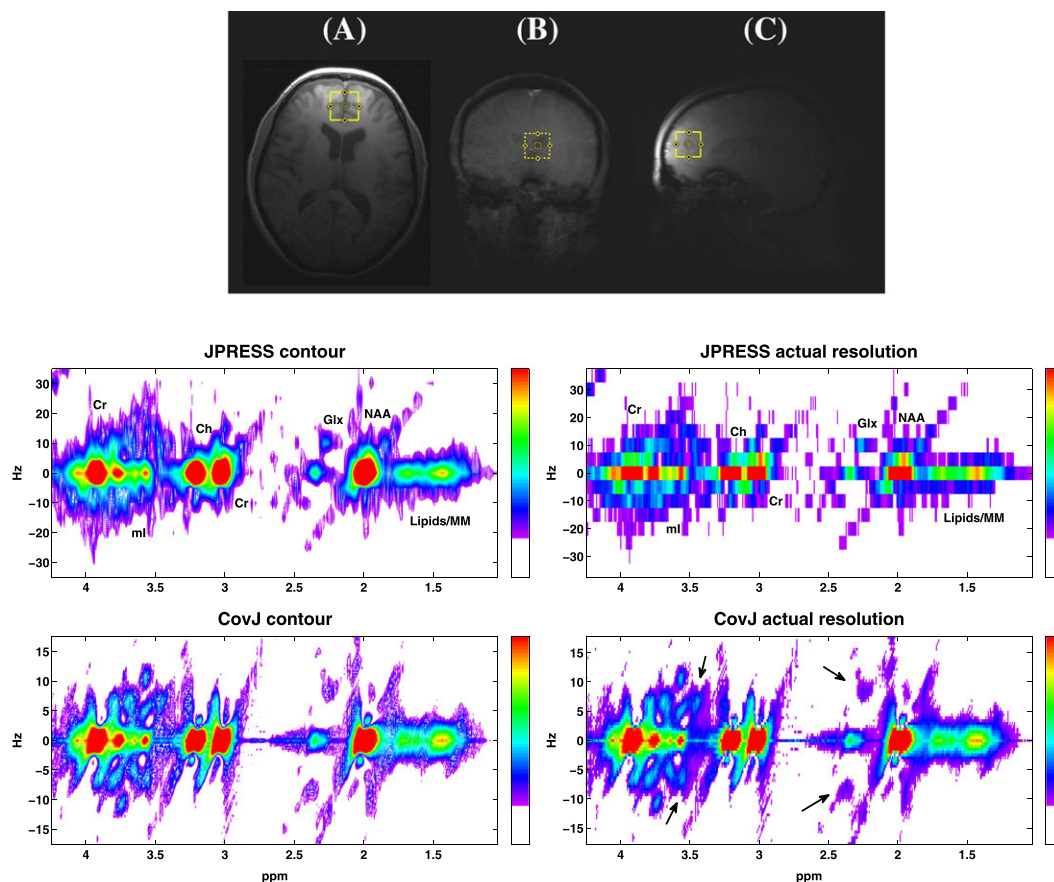
FIGURE 5 Localization is shown for the T_1-weighted MRI in A, axial, B, coronal, and C, sagittal planes for a healthy, 63 year old volunteer. JPRESS and CovJ spectra extracted and processed from this location are displayed. Contour plots are shown on the left, whereas the actual resolution for the spectra can be seen on the right. In the CovJ spectrum, J-coupled signals appear, as indicated with black arrows for Glx and mI
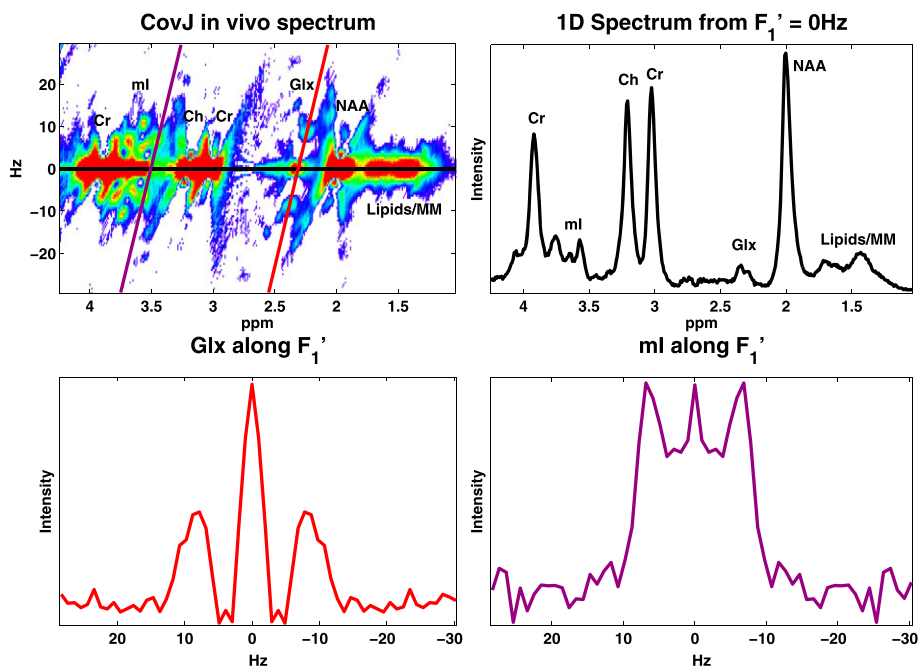
FIGURE 6 One-dimensional spectra are extracted from the CovJ spectrum seen in the top left. Spectra were extracted from $F_1' = 0$ Hz (black), the Glx peaks (red), and the mI peaks (purple)

TABLE 1 Ratios with respect to Cr3.0 are tabulated for 24 healthy volunteers (mean age = 64.7 years) using both JPRESS and CovJ methods. Data are displayed as mean values (CV% values) for all metabolites. mI/Cr3.0 was significantly higher using the CovJ method compared with the JPRESS method, and this result is explained further in the text

| Metabolite	JPRESS	CovJ
Lipids+MM	1.23(50%)	1.31(49%)
NAA	1.21(18%)	1.20(15%)
Glx	1.62(11%)	1.63(14%)
Ch	0.32(8.1%)	0.33(8.2%)
mI	0.66(8.9%)	0.75(11%)[a]

[a]$p < 0.001$

were as follows: 0.996 for Lipids + MM, 0.959 for NAA, 0.963 for Glx, 0.977 for Cr3.0, 0.979 for Ch, and 0.877 for mI. In addition, all correlation coefficients were found to be significant ($p < 0.001$). These findings demonstrate that the CovJ method is essentially as effective as JPRESS in detecting changes in metabolic levels when peak integration is used for quantitation.

In addition to peak integration, prior-knowledge fitting was used to quantify Glu and GABA ratios with respect to Cr3.0 for both the JPRESS and CovJ methods. Figure 7 shows the 2.15–2.65 ppm regions for the acquired CovJ spectrum, the fit of the CovJ spectrum, and the residual. Also, GABA and Glu ratios with respect to Cr3.0 are shown for all 24 healthy subjects using ProFit to quantify the JPRESS data and using Cov-SEHAR to quantify the CovJ data. The mean (CV%) values for GABA were 0.41 (50%) using ProFit and 0.14 (31%) using Cov-SEHAR. For Glu, the mean (CV%) values were 1.21 (18%) using ProFit and 1.27 (24%) using Cov-SEHAR. While no differences were seen between the two quantitation methods for quantifying Glu, a Student's t-test demonstrated significant differences between the GABA results ($p < 0.001$).

4 | DISCUSSION

The covariance J-resolved method, which implements the covariance transformation for processing JPRESS data, has been described and applied in vivo at 3T. The theoretical framework for this technique is similar to previously discussed covariance NMR theory,[18,19] and focuses on the relationship between FIDs across the indirect temporal direction, t_1. Spectral points along F_2 that are closely related will have similar phase modulations across the t_1 FID depending on the experiment performed. Applying a covariance transformation to these points will therefore result in cross-peaks, or off-diagonal peaks, with higher amplitudes. This is in stark contrast to F_2 points, which are unrelated, as the covariance values of these t_1 FIDs will usually be close to zero. Experiments such as TOCSY, which have high correlation values between F_2 points, are ideal for utilizing the full potential of the covariance transformation.
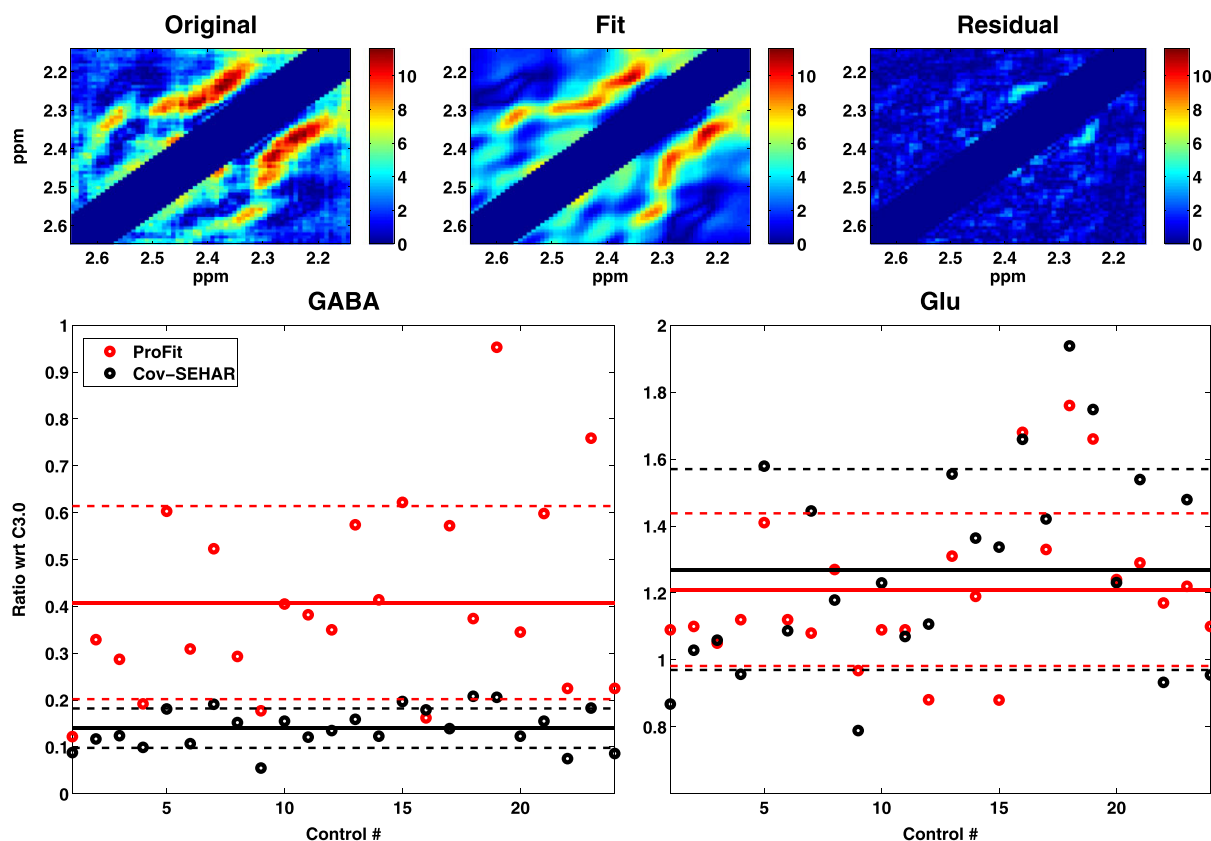
FIGURE 7 The fit results using Cov-SEHAR are shown for a healthy control (age = 63 years). The original data acquired, the fit, and the residual are shown at the top. Resulting GABA and Glu ratios with respect to Cr3.0 (wrt Cr3.0) are shown for all 24 healthy controls. ProFit results are displayed in red, whereas Cov-SEHAR results are displayed in black. The solid lines show the means of the data, and the dashed lines indicate the standard deviations of the data. While no statistical difference was found when comparing the Glu results, a Student's t-test showed significant differences ($p < 0.001$) between the ProFit and Cov-SEHAR results for GABA

However, by employing a maximum-echo sampling scheme[16] it is also possible to use the covariance transformation on J-resolved spectra, as demonstrated in this study. This sampling method not only improves overall sensitivity, but also induces a phase modulation along t_1 that can be utilized to perform the covariance transformation effectively. This phase term is introduced due to the fact that chemical shift is not refocused when using maximum-echo sampling. Following the covariance transformation, it is possible to tilt the spectrum to the correct orientation by applying a phase modulation term, τ_2, in the mixed (F_2, t_2') dimension. This process does not result in any distortions to the line shapes; however, the spectral bandwidth is reduced by a factor of two. It is important to note that if the covariance transformation is applied after tilting the data by τ_1 then several false cross-peaks form, due to the modified phase evolution along t_1. Fortunately, the processing steps described in Figure 1 lead to an S_{cov} matrix that is more representative of a JPRESS spectrum.

Simulations were used to show that the JPRESS and CovJ spectra have similarities, as well as differences originating from the unique processing steps of each method. The diagonal peaks ($F_1/F_1' = 0$ Hz) are very similar when comparing the two methods, which is apparent in Figure 5. However, an additional signal is added to the CovJ diagonal, due to the fact that C_{ii} points will have higher amplitudes than C_{ij} points according to Equation 1. For metabolites such as Lac, seen in Figure 2, the collapse of signal along $F_1' = 0$ Hz may be a potential disadvantage of the CovJ method. The mechanism behind cross-peak formation for the CovJ method, where the relationship between F_2 points is spread into the F_1' dimension, has different effects depending on the strength of coupling. For strongly coupled spin systems,[11] stronger cross-peaks are observed in Figure 2, whereas weakly coupled spin systems show suppressed cross-peak amplitudes. This is best demonstrated by mI (strong coupling) and Lac (weak coupling). Therefore, the CovJ method, in addition to improving spectral resolution, may also provide a unique contrast to the J-resolved spectrum based on coupling strength.

When comparing the cross-peaks from the two methods, it is important to note that the JPRESS indirect spectral dimension, F_1, can be used to compute J-coupling between different resonances in high-resolution NMR directly. Due to the mathematical nature of the covariance transformation, the physical value of J coupling is lost in the F_1' dimension. Thus, the results suggest that the CovJ method is not appropriate for high-resolution NMR, since the primary focus in this field is actually to quantify the J-coupling constants. For in vivo MRS, accurate J-coupling constants are not measurable unequivocally, due to experimental complications, including line broadening and low signal-to-noise ratios. Also, many metabolites of interest are strongly coupled spin systems, and therefore cross-peaks may reside very close to the diagonal peaks. For in vivo purposes, the spread of signal is more important than the physical J-coupling constant for the JPRESS method. Even though cross-peak structures are different between

the JPRESS and CovJ techniques, CovJ still performs the primary responsibility of achieving spectral dispersion along the indirect dimension, as seen in Figure 5.

From a quantitative standpoint, it is apparent from the in vivo peak integration results that the two methods yield similar metabolic concentration and ratio values. Table 1 demonstrates that the ratios for most metabolites are nearly identical between the two methods, with the exception of mI. The increased mI ratio for CovJ is easily rationalized by observing that for in vivo spectra, seen in Figure 5, additional off-diagonal peaks are formed in the mI region at $F_1' = \pm 5$ Hz and $F_1' = \pm 7$ Hz. Since these peaks lie in the integration region for mI, the CovJ mI ratios are elevated compared with the JPRESS mI ratios. In addition, the r^2 correlation values associated with metabolite concentrations are very high, implying a strong linear relationship between the quantitative results of the two methods.

Since initial in vivo quantitative comparisons yield similar results, it is important to note that there are several potential advantages of the CovJ method that make it an attractive alternative, or addition, to the standard JPRESS method. Of course, the improved resolution along the indirect dimension is the main highlight of the CovJ technique. In order to have comparable resolution using JPRESS, the indirect dimensions would have to be zero-filled to t_1 points = 1024. A direct comparison, seen in Figure 3, demonstrates that zero-filling to this resolution results in severe spectral ringing along the F_1 domain; this is a well-known drawback of the zero-filling method.[17] As mentioned above, CovJ off-diagonal peaks may change shape and F_1' location as a function of metabolite concentration, which is shown in Figure 4. This is advantageous because the same peaks can now be modeled using additional parameters, such as distance between cross-peaks, which may elucidate true metabolite concentrations further. Therefore, it may be possible to refine quantitation further using these off-diagonal peak characteristics.

To investigate this potential advantage, the Cov-SEHAR prior-knowledge quantitation method was developed to quantify Glu and GABA from CovJ spectra and was compared with the standard ProFit algorithm, which fits JPRESS spectra.[30] ProFit utilizes both non-linear and linear fitting to model the 2D spectrum in order to provide accurate metabolite ratios with respect to Cr3.0. Since the addition of metabolites using CovJ is non-linear, Cov-SEHAR fits all parameters non-linearly, including concentration values. Furthermore, the spectral masking matrix ($\mathcal{M}$) aids in focusing the fit entirely on the cross-peaks of interest, which in this case were the cross-peaks that lie in between 2.15 and 2.65 ppm. Figure 7 demonstrates that Glu results between the two quantitation methods are very similar. However, significant differences arise between the ProFit and Cov-SEHAR results for GABA. From these pilot findings, it appears that Cov-SEHAR results may be more stable when fitting data of varying spectral quality, demonstrated by lower *CV%* values. The Cov-SEHAR results are similar to previous reports regarding GABA in the human brain,[30,34,35] whereas the ProFit results seem to be over-estimated. It is important to note that the original ProFit was used in this study, and a more detailed comparison study between ProFit 2.0[31] and a refined Cov-SEHAR method is necessary before any definite conclusions can be drawn.

An important aspect of the CovJ method is that spectra are obtained using the same data necessary to produce JPRESS results: $a(t_2, t_1)$. Therefore, no extra acquisition time and minimal additional processing steps are necessary to produce CovJ data. Thus, CovJ may be used as a subset of an existing JPRESS study, and can be used to validate findings from JPRESS quantitation without impacting the study protocol. In addition to J-resolved spectroscopy, the CovJ processing method can readily be applied to the constant-time PRESS (CT-PRESS) acquisition.[15] The only modification necessary for implementing this method is that S' will be used as the final S_{cov} matrix, since tilting is unnecessary for displaying the CT-PRESS spectra. Also, the CovJ method can be applied to multi-voxel J-resolved acquisitions, including experiments incorporating acceleration techniques,[36,37] on a voxel-by-voxel basis. Future studies will focus on utilizing the additional information provided in CovJ spectra to enhance 2D JPRESS quantitation further, and will apply the CovJ method to multi-voxel J-resolved acquisitions.

5 | CONCLUSION

A novel method for improving spectral resolution along the indirect dimension has been demonstrated for the single-voxel J-resolved spectroscopy experiment. Simulation and in vivo results have shown that, while a number of qualitative differences exist between the two methods, including off-diagonal peak structure, the CovJ technique is still quantitatively similar to the JPRESS method when using peak integration. With the development of more advanced prior-knowledge fitting techniques, a combination of ProFit and Cov-SEHAR fitting may aid in the quantitation of metabolites in the future.

REFERENCES

1. Soares D, Law M. Magnetic resonance spectroscopy of the brain: Review of metabolites and clinical applications. *Clin Radiol*. 2009;64:12–21.
2. Costello L, Franklin R, Narayan P. Citrate in the diagnosis of prostate cancer. *The prostate*. 1999;38:237–245.
3. Fischbach F, Bruhn H. Assessment of in vivo 1H magnetic resonance spectroscopy in the liver: A review. *Liver Int*. 2008;28:297–307.
4. Boesch C, Slotboom J, Hoppeler H, Kreis R. In vivo determination of intra-myocellular lipids in human muscle by means of localized 1H-MR-spectroscopy. *Magn Reson Med*. 1997;37:484–493.

5. Bolan PJ, Nelson MT, Yee D, Garwood M. Imaging in breast cancer: Magnetic resonance spectroscopy. *Breast Cancer Res.* 2005;7:149–152.

6. Bottomley PA. Spatial localization in NMR spectroscopy in vivo. *Ann New York Acad Sci.* 1987;508:333–348.

7. Ramadan S, Lin A, Stanwell P. Glutamate and glutamine: A review of in vivo MRS in the human brain. *NMR Biomed.* 2013;26:1630–1646.

8. Provencher SW. Estimation of metabolite concentrations from localized in vivo proton NMR spectra. *Magn Reson Med.* 1993;30:672–679.

9. Mescher M, Merkle H, Kirsch J, Garwood M, Gruetter R. Simultaneous in vivo spectral editing and water suppression. *NMR Biomed.* 1998;11:266–272.

10. Aue W, Bartholdi E, Ernst RR. Two-dimensional spectroscopy. Application to nuclear magnetic resonance. *J Chem Phys.* 1976;64:2229–2246.

11. Ryner LN, Sorenson JA, Thomas MA. Localized 2D xJ-resolved 1 H MR spectroscopy: Strong coupling effects *in vitro* and in vivo. *Magn Reson Imaging.* 1995;13:853–869.

12. Kreis R, Boesch C. Spatially localized, one-and two-dimensional NMR spectroscopy and in Vivo application to human muscle. *J Magn Reson Ser B.* 1996;113:103–118.

13. Thomas MA, Ryner LN, Mehta MP, Turski PA, Sorenson JA. Localized 2D J-resolved H MR spectroscopy of human brain tumors in vivo. *J Mag Reson Imaging.* 1996;6:453–459.

14. Thomas MA, Yue K, Binesh N, et al. Localized two-dimensional shift correlated MR spectroscopy of human brain. *Magn Reson Med.* 2001;46:58–67.

15. Dreher W, Leibfritz D. Detection of homonuclear decoupled in vivo proton NMR spectra using constant time chemical shift encoding: CT-PRESS. *Magn Reson Imaging.* 1999;17:141–150.

16. Schulte RF, Lange T, Beck J, Meier D, Boesiger P. Improved two-dimensional J-resolved spectroscopy. *NMR Biomed.* 2006;19:264–270.

17. Bartholdi E, Ernst R. Fourier spectroscopy and the causality principle. *J Mag Reson.* 1973;11:9–19.

18. Brüschweiler R, Zhang F. Covariance nuclear magnetic resonance spectroscopy. *J Chem Phys.* 2004;120:5253–5260.

19. Brüschweiler R. Theory of covariance nuclear magnetic resonance spectroscopy. *J Chem Phys.* 2004;121:409–414.

20. Zhang F, Brüschweiler R. Indirect covariance NMR spectroscopy. *J Amer Chem Soc.* 2004;126:13180–13181.

21. Zhang F, Brüschweiler R. Spectral deconvolution of chemical mixtures by covariance NMR. *Chem Phys Chem.* 2004;5:794–796.

22. Trbovic N, Smirnov S, Zhang F, Brüschweiler R. Covariance NMR spectroscopy by singular value decomposition. *J Mag Reson.* 2004;171:277–283.

23. Snyder DA, Zhang F, Brüschweiler R. Covariance NMR in higher dimensions: Application to 4D NOESY spectroscopy of proteins. *J Biomol NMR.* 2007;39:165–175.

24. Snyder DA, Xu Y, Yang D, Brüschweiler R. Resolution-enhanced 4D 15N/13C NOESY protein NMR spectroscopy by application of the covariance transform. *J Amer Chem Soc.* 2007;129:14126–14127.

25. Thomas MA, Iqbal Z, Sarma MK, Nagarajan R, Macey PM, Huda A. 2-D MR spectroscopy combined with 2-D/3-D spatial encoding. *eMagRes.* 2016;5:1039–1060.

26. Macura S, Brown LR. Improved sensitivity and resolution in two-dimensional homonuclear J-resolved NMR spectroscopy of macromolecules. *J Magn Reson.* 1983;53:529–535.

27. Smith S, Levante T, Meier BH, Ernst RR. Computer simulations in magnetic resonance. An object-oriented programming approach. *J Mag Reson Ser A.* 1994;106:75–105.

28. Govindaraju V, Young K, Maudsley AA. Proton NMR chemical shifts and coupling constants for brain metabolites. *NMR Biomed.* 2000;13:129–153.

29. Ogg RJ, Kingsley R, Taylor JS. WET, a T 1-and B 1-insensitive water-suppression method for in vivo localized 1 H NMR spectroscopy. *Journal of Magnetic Resonance, Series B.* 1994;104:1–10.

30. Schulte RF, Boesiger P. ProFit: Two-dimensional prior-knowledge fitting of J-resolved spectra. *NMR Biomed.* 2006;19:255–263.

31. Fuchs A, Boesiger P, Schulte RF, Henning A. ProFit revisited. *Magn Reson Med.* 2014;71:458–468.

32. Iqbal Z, Wilson NE, Thomas MA. 3D spatially encoded and accelerated TE-averaged echo planar spectroscopic imaging in healthy human brain. *NMR Biomed.* 2016;29:329–339.

33. Van Belle G, Fisher LD, Heagerty PJ, Lumley T. *Biostatistics: A methodology for the health sciences.* Hoboken, New Jersey, USA: John Wiley & Sons; 2004.

34. Prescot AP, Renshaw PF. Two-dimensional J-resolved proton MR spectroscopy and prior knowledge fitting (ProFit) in the frontal and parietal lobes of healthy volunteers: Assessment of metabolite discrimination and general reproducibility. *Journal of Magnetic Resonance Imaging.* 2013;37:642–651.

35. Ernst J, Böker H, Hättenschwiler J, et al. The association of interoceptive awareness and alexithymia with neurotransmitter concentrations in insula and anterior cingulate. *Soc Cogn Affect Neurosci.* 2013;9:857–863.

36. Furuyama JK, Wilson NE, Burns BL, Nagarajan R, Margolis DJ, Thomas MA. Application of compressed sensing to multidimensional spectroscopic imaging in human prostate. *Magn Reson Med.* 2012;67:1499–1505.

37. Wilson NE, Iqbal Z, Burns BL, Keller M, Thomas MA. Accelerated five-dimensional echo planar J-resolved spectroscopic imaging: Implementation and pilot validation in human brain. *Magn Reson Med.* 2016;75:42–51.